

Accepted for publication at the IFAC World Congress 2023

©2023 the authors. This work has been accepted to IFAC for publication under a Creative Commons Licence
CC-BY-NC-ND

arXiv:2304.09334v1 [eess.SY] 18 Apr 2023

Model-Free Control Design Procedure Applied to Lateral Vehicle Control

Marcos Moreno-Gonzalez* Jorge Villagra*

* Centre for Automation and Robotics (CAR), CSIC - Universidad
Politécnica de Madrid, ctra. de Campo Real, km 0,200, 28500 Arganda
del Rey, Spain, (e-mail: {marcos.moreno, jorge.villagra}@csic.es).

Abstract: Model-Free Control has proven its performance in a wide variety of systems. Although its adequate tuning can be achieved using the knowledge of the system and optimization-based approaches, there is not yet a systematic design procedure for this kind of control scheme. In this paper, a non-iterative Three Term Controller tuning procedure is adapted and extended to fit Model-free controllers' structure. This procedure is successfully applied to design the lateral control of an automated car with realistic performance requirements.

Keywords: Controller Design, Model-free control, Autonomous vehicles, Stability and stabilization

1. INTRODUCTION

Model-Free Control (MFC) (Fliess and Join, 2013) has gained attention over the last years as a control technique able to successfully regulate complex systems that are time-varying or non-linear, e.g., Fliess and Join (2021), Villagra et al. (2009) and Villagra et al. (2020) are some examples that show this potential. Variations of the original control structure can also be found in the literature, such as Wang et al. (2020) and Moreno-Gonzalez et al. (2022). However, although some recent works propose different solutions (Yahagi and Kajiwara, 2022; Hegedüs et al., 2022), the design of these *intelligent* controllers is still an open problem.

In this paper, a new control design procedure for regulators under the Model-Free Control paradigm is presented. The proposed algorithm consists on the adaptation of the discrete Three Term Controller design procedure collated in Bhattacharyya et al. (2018). It is based on the root-counting and phase unwrapping formulas for discrete-time systems detailed in Keel and Bhattacharyya (2002), and allows the designer to obtain the stability region of the controller given an approximate model of the system.

To evaluate the potential of the MFC design procedure, the lateral control of an automated car is studied, applying appropriate restrictions for the control design and using a realistic vehicle simulator.

The rest of the paper is structured as follows. Section 2 presents the Three Term Controller design procedure which is later adapted to MFC. A brief introduction to Model-Free Control is presented in Section 3. Section 4 details the proposed adaptation from PID design to Model-Free Control design. An illustrative example and the results from simulation are presented in Section 5. Finally, concluding remarks and references can be found in the last section.

2. THREE TERM CONTROLLER DESIGN PROCEDURE

This section briefly explains the Three Term Controller design procedure that provides a stabilizing set of control parameters for a given plant model that will be used in this work. The design procedure is taken from Bhattacharyya et al. (2018) and the references therein, where a complete description of the algorithm can be found.

Consider a discrete-time system $G(z) = N(z)/D(z)$ where $N(z)$ and $D(z)$ are real polynomials, being $\deg[D(z)] = n_1$ and $\deg[N(z)] = l_1 \leq n_1$. The plant is controlled by a Two Term Controller (which is similar to a PI controller):

$$C_{PI}(z) = K_1 \frac{z - K_2}{z - 1} \quad (1)$$

or a Three Term Controller (similar to a PID controller):

$$C_{PID}(z) = \frac{K_2 z^2 + K_1 z + K_0}{z(z - 1)} \quad (2)$$

The characteristic equation of the closed-loop system $\delta(z)$ can be expressed for each controller as follows:

$$\delta_{PI}(z) = (z - 1) \cdot D(z) + K_1(z - K_2) \cdot N(z)$$

$$\delta_{PID}(z) = z(z - 1) \cdot D(z) + (K_2 z^2 + K_1 z + K_0) \cdot N(z)$$

The parameters that stabilize the closed-loop system, i.e., the stability region, can be found following these steps:

- 1) Define $N(z)$ and $D(z)$ and find their Tchebychev representation:

$$D(z) = \sum_{k=0}^{n_1} a_k \cdot z^k; \quad N(z) = \sum_{k=0}^{l_1} b_k \cdot z^k$$

$$N(z) \Big|_{z=e^{j\theta}} = N(e^{j\theta}) \Big|_{\cos \theta=u} = R_N(u) + j\sqrt{1-u^2}T_N(u)$$

$$D(z) \Big|_{z=e^{j\theta}} = D(e^{j\theta}) \Big|_{\cos \theta=u} = R_D(u) + j\sqrt{1-u^2}T_D(u)$$

$$R_D(u) = \sum_{k=1}^{n_1} a_k \cdot c_k(u) + a_0; \quad T_D(u) = \sum_{k=1}^{n_1} a_k \cdot s_k(u)$$

$$R_N(u) = \sum_{k=1}^{l_1} b_k \cdot c_k(u) + b_0; \quad T_N(u) = \sum_{k=1}^{l_1} b_k \cdot s_k(u)$$

where c_k and s_k are defined in Table 1.

k	$c_k(u)$	$s_k(u)$
1	$-u$	1
2	$2u^2 - 1$	$-2u$
3	$-4u^3 + 3u$	$4u^2 - 1$
4	$8u^4 - 8u^2 + 1$	$-8u^3 + 4u$
5	$-16u^5 + 20u^3 - 5u$	$16u^4 - 12u^2 + 1$
\vdots	\vdots	\vdots

Table 1. Generalized Tchebychev polynomials

- Define $\nu(z)$ for each controller from the corresponding characteristic equation and find its Tchebychev representation:

$$\begin{aligned} \nu_{PI}(z) &= \delta(z)N(z^{-1}) \\ &= R(u, K_{1,2}) + j\sqrt{1-u^2} \cdot T(u, K_1) \end{aligned}$$

$$\begin{aligned} R(u, K_{1,2}) &= -(u+1)P_1(u) - (1-u^2)P_2(u) \\ &\quad - K_1(u+K_2)P_3(u) \end{aligned} \quad (3)$$

$$T(u, K_1) = K_1P_3(u) + P_1(u) - (u+1)P_2(u)$$

$$\begin{aligned} \nu_{PID}(z) &= z^{-1}\delta(z)N(z^{-1}) \\ &= R(u, K_{1,2,3}) + j\sqrt{1-u^2} \cdot T(u, K_3) \end{aligned}$$

$$\begin{aligned} R(u, K_{1,2,3}) &= -(u+1)P_1(u) - (1-u^2)P_2(u) \\ &\quad - [(2K_2 - K_3)u - K_1]P_3(u) \end{aligned} \quad (4)$$

$$T(u, K_3) = K_3P_3(u) + P_1(u) - (u+1)P_2(u)$$

where K_3 is defined as $K_3 \triangleq K_2 - K_0$.

Note that $T(\cdot)$ only depends on one control parameter, either K_1 or K_3 .

Obtain $P_1(u)$, $P_2(u)$ and $P_3(u)$:

$$P_1(u) = R_D(u)R_N(u) + (1-u^2)T_D(u)T_N(u)$$

$$P_2(u) = R_N(u)T_D(u) - R_D(u)T_N(u)$$

$$P_3(u) = R_N^2(u) + (1-u^2)T_N^2(u)$$

- Calculate the signature of $\nu(z)$ as σ :

$$\sigma_{PI} = i_\delta + i_{N_r} - l_1$$

$$\sigma_{PID} = i_\delta + i_{N_r} - l_1 - 1$$

where i_δ and i_{N_r} are the number of roots inside the unit circle of $\delta(z)$ and $N_r(z)$ respectively, and $N_r(z)$ is defined as $N_r(z) = N(z^{-1}) \cdot z^{l_1}$. Note that all the roots of $\delta(z)$ must be inside the unit circle to ensure stability ($i_\delta = \deg[\delta(z)]$).

- Obtain the set of K_1 or K_3 as appropriate ($K_{1(3)}$) such that $T(u, K_{1(3)})$ from (3) or (4) have at least $\sigma - 1$ real different zeros of odd multiplicity when $u \in (-1, 1)$. For this purpose, root locus can be applied as $T(\cdot)$ only depends on one parameter.
- If the set of $K_{1(3)}$ is empty, then there is no stabilizing set for the system with the type of controller chosen.

For each $K_{1(3)}$:

- Find the k real distinct zeros of odd multiplicity t_i of $T(u)$ ((3) or (4)) for $u \in (-1, 1)$ and arrange them as $-1 < t_1 < t_2 < \dots < t_k < +1$.
- Build the set of sequences (known as *strings*) $A_k = \{\{i_0, i_1, \dots, i_k, i_{k+1}\}\}$ where each i_j has the value -1 or 1 , k is the number of real distinct zeros of odd

multiplicity of $T(u)$ from the previous step and A_k covers all the possible combinations.

- Determine the admissible string set $I \in A_k$ in which each admissible string satisfies:

$$\sigma = \frac{\text{sgn}[T^{(p)}(-1)]}{2} \left(i_0 + 2 \sum_{j=1}^k (-1)^j i_j + (-1)^{k+1} i_{k+1} \right)$$

where p is the number of zeros of $T(u)$ in $u = -1$.

For each admissible string I_i :

- Determine the values of K_2 (and K_1 for PID) that simultaneously satisfy the inequalities:

$$R(t_j) \cdot i_t > 0 \quad \forall t = 0, 1, \dots, k, k+1$$

- Only in the PID case, obtain K_0 from $K_3 = K_2 - K_0$.

Remark 1. The stabilizing set obtained with this procedure contains all and only the control parameters that make the closed-loop system stable. However, concrete values of $K_{1(3)}$ are needed for steps 6 to 10, so a discretization has to be made which can cause a loss of information (see Fig. 1 for an illustrative example).

3. MODEL-FREE CONTROL PRINCIPLES

In Fliess and Join (2013), it is shown that the dynamics of a system can be replaced by an ultra-local model

$$y^{(n)} = F + \alpha \cdot u \quad (5)$$

in which the input u and the n th time derivative of the output y are linearly related by a constant design parameter α and the relationship is fitted by F , a variable that absorbs system disturbances and model errors. Note that n defines the order of the ultra-local model.

The control loop is typically closed by a so-called *intelligent PID* controller, iPID controller (usually iP or iPD):

$$u = \frac{1}{\alpha} \cdot \left(-F + y_r^{(n)} + K_p e + K_i \int e + K_d \dot{e} \right) \quad (6)$$

where u is the control action, suffix r stands for reference, e is the error and K_p , K_i and K_d are the PID control parameters. F is estimated in real time using an estimator \hat{F} ; the simplest one assumes it to be constant between consecutive instants and can be estimated from (5) as:

$$\hat{F}(t_k) = \hat{y}^{(n)}(t_k) - \alpha \cdot u(t_{k-1}) \quad (7)$$

where t_k is the current instant and $\hat{y}^{(n)}$ is the filtered n th time derivative of y . More elaborated estimators for discrete-time settings can be found in Sanyal (2022).

Remark 2. Note that the error dynamics derived from (5) and (6) can be expressed as $e^{(n)} + K_d \dot{e} + K_p e + K_i \int e = \hat{F} - F$. If the estimation of F is good enough ($\hat{F} \approx F$), then the system dynamics can be made asymptotically stable through an appropriate choice of the control parameters and order of the ultra-local model.

4. MFC DESIGN PROCEDURE

4.1 Justification

The developed design procedure is based on the relationship between Model-free controllers and the Three Term Controllers from Section 2.

Although MFC has advantages over PID control, both in terms of performance and robustness (cf. Li et al. (2022)), a mathematical equivalence between PI(D) and iPD control structures can be demonstrated under certain assumptions (e.g., assuming that the derivative of the output of the system is not filtered, d'Andréa Novel et al. (2010)). However, real measurements are usually filtered before derivation to prevent the control action (6) from chattering (as it depends on the derivative of the system output).

In the following sections, the equivalence between a first (second) order iPD controller and a Two (Three) Term Controller (corresponding to PI and PID controllers) is shown considering a filtered derivative of the system output, as requested in (7). This derivative can be expressed as the following operator:

$$D(z) = \frac{1}{T_s} \frac{z-1}{Cz+1-C} \quad (8)$$

where T_s is the sampling time and C is a filtering parameter, which is characterized according to the measured signal-noise ratio.

Notice that only iPD controllers are considered in this work, as they are the most usual (Fliess and Join, 2021).

4.2 First Order iPD and PI

From (6), (7) and (8), and considering a first order ultra-local model, the discrete transfer function $C_{iPD_1}(z)$ of the iPD controller, that relates the control action $U(z)$ to the error $E(z)$, can be obtained:

$$C_{iPD_1}(z) = \frac{U_{iPD_1}(z)}{E(z)} = \frac{\frac{K_p T_s C + K_d + 1}{\alpha T_s} z^2 - \frac{K_p T_s (C-1) + K_d + 1}{\alpha T_s} z}{(z-1) \cdot (Cz+1-C)} \quad (9)$$

which in turn yields:

$$C_{iPD_1}(z) = K_1 \frac{z-K_2}{z-1} \cdot \frac{z}{Cz+1-C}$$

where

$$K_1 = \frac{K_p T_s C + K_d + 1}{\alpha T_s}; \quad K_2 = \frac{K_p T_s (C-1) + K_d + 1}{\alpha T_s} \quad (10)$$

Comparing the direct loops $C_{PI}(z) \cdot G(z)$ and $C_{iPD_1}(z) \cdot G(z)$, it is obtained that controlling a system $G(z)$ with the iPD₁ controller from (9) is the same as controlling $G(z) \cdot \frac{z}{Cz+1-C}$ with the Two Term (PI) controller from (1). Additionally, an inverse relationship can be obtained from (10):

$$\frac{K_p}{\alpha} = K_1 \cdot (1-K_2); \quad \frac{K_d+1}{\alpha} = T_s K_1 \cdot (1-C+K_2 C) \quad (11)$$

Remark 3. Note that (11) is a non-linear equation in which one of the iPD control parameters is undetermined.

4.3 Second Order iPD and PID

Alternatively, if a second order ultra-local model is considered, the transfer function of the controller can be expressed as follows:

$$C_{iPD_2}(z) = z \frac{K_p T_s^2 (Cz+1-C)^2 + K_d T_s (z-1)(Cz+1-C) + (z-1)^2}{\alpha T_s^2 (z-1)(Cz+1-C)^2} \quad (12)$$

which yields:

$$C_{iPD_2}(z) = \frac{K_2 z^2 + K_1 z + K_0}{z(z-1)} \cdot \frac{z^2}{(Cz+1-C)^2}$$

where

$$\begin{aligned} K_2 &= \frac{K_p T_s^2 C^2 + K_d T_s C + 1}{\alpha T_s^2} \\ K_1 &= \frac{2K_p T_s^2 C(1-C) + K_d T_s (1-2C) - 2}{\alpha T_s^2} \\ K_0 &= \frac{K_p T_s^2 (C-1)^2 + K_d T_s (C-1) + 1}{\alpha T_s^2} \end{aligned} \quad (13)$$

As in the previous section, comparing the direct loops when Three Term (PID) and iPD₂ controllers are applied to the plant, it is obtained that controlling a system $G(z)$ with the iPD₂ from (12) is the same as controlling $G(z) \cdot \frac{z^2}{(Cz+1-C)^2}$ with the PID from (2). Additionally, there are two inverse relationships among the control parameters: the semi-linear (14) and the non-linear (15).

$$\begin{bmatrix} K_p/\alpha \\ K_d/\alpha \\ 1/\alpha \end{bmatrix} = \begin{bmatrix} 1 & 1 & 1 \\ 2T_s(1-C) & T_s(1-2C) & -2T_s C \\ T_s^2(C-1)^2 & T_s^2(C^2-C) & T_s^2 C^2 \end{bmatrix} \begin{bmatrix} K_2 \\ K_1 \\ K_0 \end{bmatrix} \quad (14)$$

$$\begin{bmatrix} T_s^2 C^2 & T_s C & -T_s^2 K_2 \\ T_s^2 2C(1-C) & T_s(1-2C) & -T_s^2 K_1 \\ T_s^2 (C-1)^2 & T_s(C-1) & -T_s^2 K_0 \end{bmatrix} \begin{bmatrix} K_p \\ K_d \\ \alpha \end{bmatrix} = \begin{bmatrix} -1 \\ 2 \\ -1 \end{bmatrix} \quad (15)$$

5. RESULTS

In this section, the Model-free controller design procedure presented in previous sections is applied to tune the lateral controller of an autonomous vehicle.

5.1 Vehicle simplified model

Vehicle's lateral dynamics are linearly modeled as proposed in Rajamani (2011):

$$\begin{bmatrix} \dot{e}_y \\ \ddot{e}_y \\ \dot{e}_\psi \\ \ddot{e}_\psi \end{bmatrix} = \begin{bmatrix} 0 & 1 & 0 & 0 \\ 0 & -\frac{2C_f l_f + 2C_r}{m v_x} & \frac{2C_f l_f + 2C_r}{m} & -\frac{2C_f l_f + 2C_r l_r}{m v_x} \\ 0 & 0 & 0 & 1 \\ 0 & \frac{2C_r l_r - 2C_f l_f}{I_z v_x} & \frac{2C_f l_f - 2C_r l_r}{I_z} & \frac{-2C_f l_f^2 - 2C_r l_r^2}{I_z v_x} \end{bmatrix} \begin{bmatrix} e_y \\ \dot{e}_y \\ e_\psi \\ \dot{e}_\psi \end{bmatrix} + \begin{bmatrix} 0 \\ \frac{2C_f}{m} \\ 0 \\ \frac{2C_f l_f}{I_z} \end{bmatrix} \delta + \begin{bmatrix} 0 \\ -\frac{2C_f l_f - 2C_r l_r}{m v_x} - v_x \\ 0 \\ -\frac{2C_f l_f^2 + 2C_r l_r^2}{I_z v_x} \end{bmatrix} \dot{\psi}_{des} \quad (16)$$

where e_y and e_ψ are the lateral and angular errors, m is the vehicle mass, v_x is the longitudinal speed, C_r and C_f are the cornering stiffness of the rear and front wheels, l_r and l_f is the distance between the center of gravity (CoG) and the rear and front axle, I_z is the yaw inertia, δ is the steering angle and $\dot{\psi}_{des}$ is the desired yaw rate. Although real vehicles are substantially more complex and have strong non-linearities and varying parameters, this model is commonly used in lateral control design (Zainal et al., 2017; Jiang and Astolfi, 2018).

The state-space model is converted to a transfer function with the vehicle parameters in Table 2. It takes the lateral

error and the steering angle as the output and input of the system, respectively, and the term related to the desired yaw rate is considered as a disturbance. The transfer function is discretized with a zero-order hold and a sample time $T_s = 0.05$ s. With the discrete-time transfer function, the procedure detailed in sections 2 and 4.3 can be applied.

Table 2. Vehicle parameters

Parameter	m	v_x	I_z	C_f	C_r	l_f	l_r
Value (IS)	1372	9.72	1990	37022.5	35900	0.98	1.48

5.2 Vehicle extended model

The model of the vehicle used in simulation tests is the same used in (Moreno-Gonzalez et al., 2022). It was designed to mimic an experimental platform (described in Artuñedo et al. (2019)) with a high degree of fidelity. For this purpose, a dynamic model with 14 degrees of freedom was considered (6 for the vehicle body motion: longitudinal, lateral, vertical, roll, pitch, and yaw; and 8 for the wheels: vertical motion and spin of each wheel).

The power-train modeling comprises three elements: (i) the engine, whose torque map has been identified from measurements taken in the experimental platform; (ii) the gearbox, that reproduces the same drive ratios and gear shifting logic of the actual vehicle; (iii) the resistance torques coming from braking system, longitudinal wind forces and gravitational forces. The tire behaviour was reproduced with the Pacejka tire model (Pacejka and Bakker, 1992).

Special attention was paid to the steering actuator modeling. An external actuation system was added in addition to the vehicle's electric power assisted steering system, which is modeled inspired on Lee et al. (2018). The main parameters of the modeled actuator, such as inertia or backlash, have been measured or identified from extensive field tests. Moreover, the small noise coming from the localization system of the experimental platform has been also characterized and included in the simulation model.

5.3 Simulation results

The derivative filter is experimentally designed to reduce the noise of the measured lateral error, resulting in $C = 4$.

Applying the Model-free controller design procedure presented in Section 4.3, i.e., obtaining the Three Term Controller stabilizing set for the equivalent system $G(z) \cdot \frac{z^2}{(Cz+1-C)^2}$ and then applying transformations (14) or (15), the iPD₂ stabilizing set for the plant model $G(z)$ is obtained, where $G(z)$ is the discrete-time representation of (16) obtained as described in Section 5.1. The stabilizing set obtained is represented in Figure 1. Note that the non-linear transformation (15) is applied because it retrieves the real control parameters (α, K_p, K_d), although the resolution of the original PID stabilizing set affects the iPD parameters.

To show that the transformation keeps the stability features assured by the initial design method, several tests are made. First, the iPD₂ stabilizing set from Fig. 1 is checked to be in fact stable through a step response simulation. It

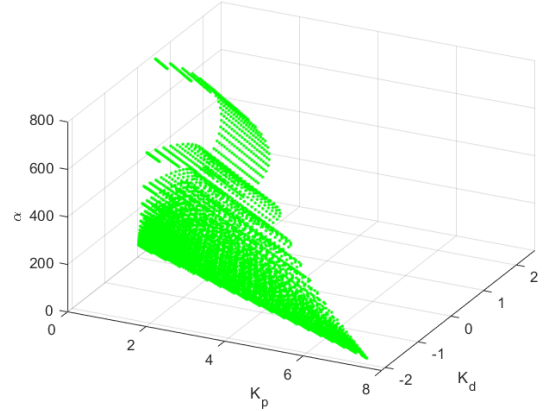


Fig. 1. iPD₂ stabilizing set obtained with (15)

is thus shown that the transformation does not worsen the stability characteristics of the closed-loop system.

Besides, two subsets of PID configurations that meet more demanding frequency and time-response restrictions (subset 1: gain margin, $GM \geq 1.5$, phase margin, $PM \geq 30$ deg; subset 2: overshoot, $OS \leq 40\%$, settling time, $ST(2\%) \leq 15$ s) are obtained and transformed into iPD₂ parameters. The restricted subsets are represented in blue in Fig. 2a and in black in Fig. 2b, respectively. The frequency-response restricted iPD₂ subset is checked to meet the restrictions given. The step response of the time-response restricted iPD subset is simulated in Fig. 3. It is thus shown that the transformation lets the second-order iPD controllers keep more strict features of the equivalent Three Term Controllers.

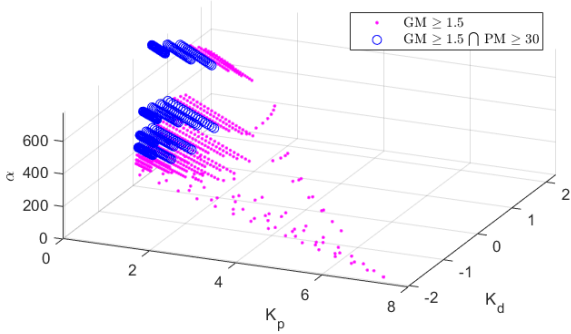
The applicability of the design method is tested on the extended vehicle model detailed in Section 5.2. Setting different frequency and time-response restrictions, different restricted subsets are obtained; e.g., the subsets that Fig. 2 show. Among those restricted subsets, four different iPD₂ configurations are chosen, which are gathered in Table 3. Note that the time-response specifications are obtained from the step response.

Table 3. iPD control parameters tested

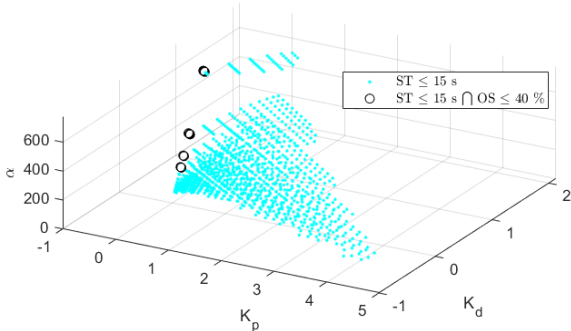
iPD Ctrl.	K_p	K_d	α	OS (%)	ST (s)	GM (dB)	PM ($^\circ$)
1	0.00093	0.043	315.7	10-20	0-10	-	-
2	0.09078	0.167	161.9	40-50	10-20	-	-
3	0.0	0.301	116.1	-	-	0-5	0-10
4	0.0	0.649	792.6	-	-	20-30	50-60

Real vehicles must not exceed certain dynamic constraints -such as in lateral acceleration (Villagra (2023)- in order to assure stability, so a step response test is unfeasible. Instead, a smooth trajectory is defined to evaluate the controller performance.

Controllers 1 and 2 are tested on the extended model using a smoothed step trajectory, setting the initial longitudinal speed of the vehicle at 35 km/h. Table 4 gathers the time-response parameters (obtained with the simplified model (16)) and with the extended model). Figure 4 shows the response of both models with controllers 1 and 2. Note that the differences between the expected and real settling time



(a) Frequency-response restricted iPD₂ subset



(b) Time-response restricted iPD₂ subset

Fig. 2. Restricted iPD₂ subsets

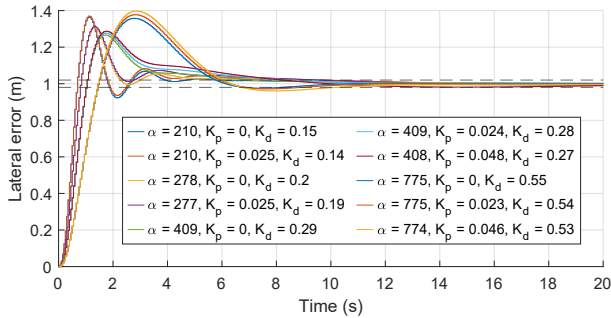


Fig. 3. Step response of restricted iPD₂ configurations

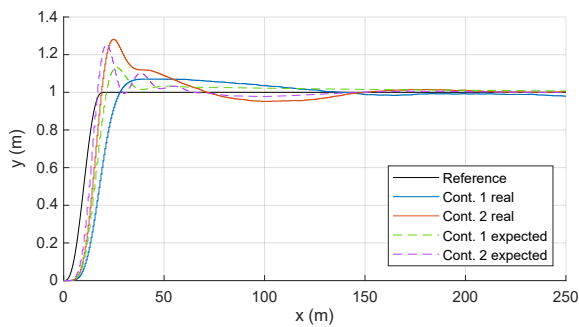


Fig. 4. Step responses of controllers 1 and 2

can be caused by the steering actuator dynamics, that are neglected in the simplified vehicle model.

On the other hand, evaluation of the gain and phase margins on the extended model is not straightforward as it is highly non-linear. Frequency-response margins are related to the absolute stability of the system, therefore it

Table 4. Time-response restrictions

iPD Controller	OS (%)		ST (5%) (s)	
	Expected	Real	Expected	Real
1	13.15	7.06	3.35	8.55
2	25.35	28.12	4.45	5.95

is tested instead by simulating the behavior of controllers 3 and 4 on test trajectories that impose different dynamic constraints on the vehicle, as can be seen in Table 5. Note that T_2 is much more demanding than T_1 in maximum speed and acceleration constraints. This test trajectories are obtained by applying the speed planning method proposed in Artuñedo et al. (2021).

Table 5. Dynamic constraints by trajectory

Trajectory	T_1	T_2
Maximum speed (km/h)	35	100
Maximum long. acceleration (m/s^2)	0.4	1.5
Maximum long. deceleration (m/s^2)	0.7	2.0
Maximum lat. acceleration (m/s^2)	1.0	4.0

Fig. 5 shows the performance of controllers 3 and 4 when applied on the extended model for test trajectories T_1 and T_2 . As can be seen, controller 3 tracks better trajectory T_1 , but becomes unstable when the speed increases in T_2 (simulation is stopped when the lateral error exceeds 3m); however, although controller 4 has worse tracking performance in T_1 , it remains stable even when the speed is high in T_2 . This results show that controller 3 is less stable than controller 4, as it was specified by design.

CONCLUDING REMARKS

The aim of this work was to develop a design procedure to obtain the set of stabilizing MFC controllers and, among them, those that meet given frequency and time-response specifications.

The proposed algorithm, a non-linear adaptation of the Three Term Controller design procedure in Bhattacharyya et al. (2018), is able to preserve all the features of the original procedure, including frequency-response restrictions (gain and phase margins) and time-response restrictions (overshoot and settling time), giving the designer a powerful tool to design MFC controllers when a model of the system is available.

The proposed MFC tuning mechanism has been successfully applied to the design of lateral controllers for autonomous vehicles. Future work will address the design of MFC regulators for continuous-time systems without discretization.

REFERENCES

- Artuñedo, A., Godoy, J., and Villagra, J. (2019). A decision-making architecture for automated driving without detailed prior maps. In *2019 IEEE Intelligent Vehicles Symposium (IV)*, 1645–1652. IEEE.
- Artuñedo, A., Villagra, J., and Godoy, J. (2021). Jerk-limited time-optimal speed planning for arbitrary paths. *IEEE Trans. on Intelligent Transport. Systems*, 1–15.
- Bhattacharyya, S.P., Datta, A., and Keel, L.H. (2018). *Linear control theory: structure, robustness, and optimization*. CRC press.

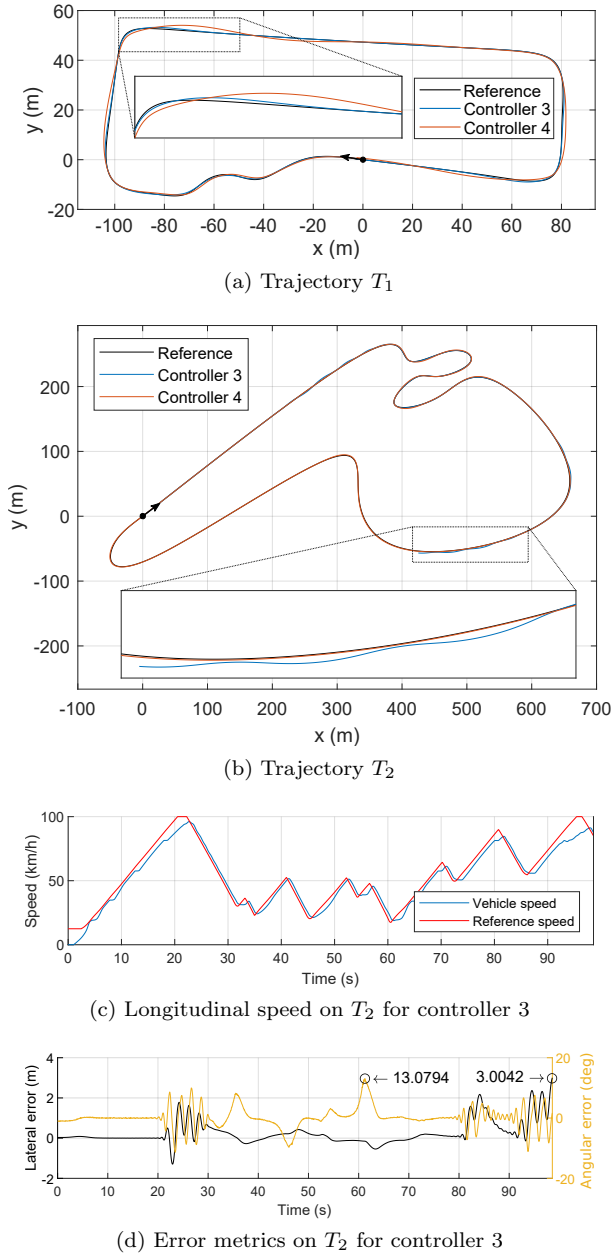


Fig. 5. Performance of controllers 3 and 4 on the benchmark trajectories

d'Andréa Novel, B., Fliess, M., Join, C., Mounier, H., and Steux, B. (2010). A mathematical explanation via “intelligent” PID controllers of the strange ubiquity of PIDs. In *18th Mediterranean Conference on Control and Automation, MED'10*, 395–400. IEEE.

Fliess, M. and Join, C. (2013). Model-free control. *International Journal of Control*, 86(12), 2228–2252.

Fliess, M. and Join, C. (2021). An alternative to proportional-integral and proportional-integral-derivative regulators: Intelligent proportional-derivative regulators. *Intl. J. of Robust and Nonlinear Ctrl.*, 1–13.

Hegedűs, T., Fényes, D., Németh, B., Szabó, Z., and Gáspár, P. (2022). Design of model free control with tuning method on ultra-local model for lateral vehicle control purposes. In *2022 American Control Conf.*, 4101–4106. IEEE.

Jiang, J. and Astolfi, A. (2018). Lateral control of an autonomous vehicle. *IEEE Transactions on Intelligent Vehicles*, 3(2), 228–237.

Keel, L. and Bhattacharyya, S. (2002). Root counting, phase unwrapping, stability and stabilization of discrete time systems. *Linear Algebra Appl.*, 351, 501–518.

Lee, D., Kim, K.S., and Kim, S. (2018). Controller design of an electric power steering system. *IEEE Trans. on Ctrl. Systems Tech.*, 26(2), 748–755.

Li, W., Yuan, H., Li, S., and Zhu, J. (2022). A revisit to model-free control. *IEEE Transactions on Power Electronics*, 37(12), 14408–14421.

Moreno-Gonzalez, M., Artuñedo, A., Villagra, J., Join, C., and Fliess, M. (2022). Speed-adaptive model-free lateral control for automated cars. In *Joint 8th IFAC Symposium on System Structure and Control, 17th IFAC Workshop on Time Delay Systems, 5th IFAC Workshop on Linear Parameter Varying Systems, IFAC 2022*.

Pacejka, H. and Bakker, E. (1992). The magic formula tyre model. *Vehicle System Dynamics*, 21, 1–18.

Rajamani, R. (2011). *Vehicle dynamics and control*. Springer Science & Business Media.

Sanyal, A. (2022). Discrete-time data-driven control with hölder-continuous real-time learning. *International Journal of Control*, 95(8), 2175–2187.

Villagra, J. (2023). Interplay between decision and control. In *Decision-Making Techniques for Autonomous Vehicles*, 193–213. Elsevier.

Villagra, J., d'Andréa Novel, B., Choi, S., Fliess, M., and Mounier, H. (2009). Robust stop-and-go control strategy: an algebraic approach for non-linear estimation and control. *Intl. J. of Vehicle Auton. Syst.*, 7(3-4), 270–291.

Villagra, J., Join, C., Haber, R., and Fliess, M. (2020). Model-free control for machine tools. In *21st IFAC World Congress, IFAC 2020*.

Wang, H., Xu, H., Tian, Y., and Tang, H. (2020). α -variable adaptive model free control of irehave upperlimb exoskeleton. *Adv. in Eng. Software*, 148, 102872.

Yahagi, S. and Kajiwara, I. (2022). Non-iterative data-driven tuning of model-free control based on an ultralocal model. *IEEE Access*, 10, 72773–72784.

Zainal, Z., Rahiman, W., and Baharom, M. (2017). Yaw rate and sideslip control using PID controller for double lane changing. *J. Telec. Electr. Comp. Eng.*, 9, 99–103.